AGU ADVANCING EARTH AND SPACE SCIENCE

Geophysical Research Letters

RESEARCH LETTER
10.1029/2020GL089512

Key Points:
- Only the Western North Pacific has robust correlations between actual and potential TC intensity
- Correlations in the North Atlantic are sensitive to the time period considered
- Potential intensity variability is driven by both SST and outflow temperature variability

Supporting Information:
- Supporting Information S1

Correspondence to:
A. A. Wing,
awing@fsu.edu

Citation:
Shields, S., Wing, A. A., & Gilford, D. M. (2020). A global analysis of interannual variability in potential and actual tropical cyclone intensities. *Geophysical Research Letters*, *47*, e2020GL089512. https://doi.org/10.1029/2020GL089512

Received 30 JUN 2020
Accepted 22 AUG 2020
Accepted article online 9 SEP 2020

A Global Analysis of Interannual Variability in Potential and Actual Tropical Cyclone Intensities

Shannon Shields[1], Allison A. Wing[1], and Daniel M. Gilford[2,3]

[1]Department of Earth, Ocean and Atmospheric Science, Florida State University, Tallahassee, FL, USA, [2]Department of Earth and Planetary Sciences, Rutgers University, New Brunswick, NJ, USA, [3]Institute of Earth, Ocean, and Atmospheric Sciences, Rutgers University, New Brunswick, NJ, USA

Abstract We examine the relationship between interannual variability of potential intensity (PI) and tropical cyclone (TC) actual intensity (AI) and the factors contributing to this variability across all global ocean basins. Using best-track data and three reanalysis products from 1980–2016, we find that the Western North Pacific is the only basin that yields consistently significant correlations between AI and PI sampled along the TC tracks. In contrast to a previous study, the North Atlantic does not yield statistically significant correlations. This is because the correlation between AI and PI in the North Atlantic is sensitive to the length of the time period considered and the individual years within that time period. Both thermodynamic efficiency and air-sea disequilibrium contribute to interannual variability in along-track PI.

1. Introduction

Potential intensity (PI) is the maximum possible intensity a tropical cyclone (TC) can achieve at steady state in a given thermodynamic environment (Bister & Emanuel, 1998; Emanuel, 1986). Even though most TCs do not reach their PI due to landfall, vertical wind shear, dry air entrainment (Tang & Emanuel, 2010), ocean coupling (Emanuel, 2015; Huang et al., 2015; Lin et al., 2013), and other factors not accounted for in PI theory, observations and model simulations show a strong link between PI and actual TC intensity (Emanuel, 2000; Gilford et al., 2019; Kossin & Camargo, 2009; Strazzo et al., 2015; Wang et al., 2014; Wing et al., 2007). Therefore, it is useful to view variability and change in actual TC intensity through the lens of PI variability (Sobel et al., 2016). Climate models from the Coupled Model Intercomparison Projects (CMIP3 and CMIP5) and physical arguments agree that PI should increase with future global warming, with the largest PI increases over the tropical Atlantic and Pacific (Camargo, 2013; Emanuel & Sobel, 2013; Yu et al., 2010). Thus, understanding variability in PI on a variety of time scales, and the factors that contribute to it, is of great importance. Recent studies have investigated the relative contribution of sea surface temperature (SST) and upper tropospheric temperature to changes in PI in idealized models (Ramsay, 2013; Wang et al., 2014) and on decadal (Camargo et al., 2013; Emanuel et al., 2013; Kossin, 2015; Polvani et al., 2016; Vecchi & Soden, 2007; Vecchi et al., 2013; Wing et al., 2015), interannual (Wing et al., 2015), and seasonal time scales (Gilford et al., 2017, 2019). While many studies have examined decadal PI trends (Emanuel et al., 2013; Free et al., 2004; Kossin, 2015; Wing et al., 2015), only a few have examined PI interannual variability (Kossin & Camargo, 2009; Wing et al., 2007). Additionally, most studies have examined basin-averaged PI (Emanuel et al., 2013; Gilford et al., 2017; Wing et al., 2015). However, in order to conduct a true test of PI theory, potential and actual intensity (AI) should be compared along actual TC tracks (Emanuel, 2000; Gilford et al., 2019; Wing et al., 2007).

The objective of this study is to analyze the relationship between the interannual variability of potential and actual TC intensity sampled along-track and the factors contributing to that variability. We extend the analysis of Wing et al. (2007) by using multiple modern reanalysis products and examining all global TC basins, and we improve on the analysis of Wing et al. (2015) by considering along-track rather than basin-averaged PI.

2. Data

Observed TC track and intensity data are derived from NOAA's National Hurricane Center (NHC) for the North Atlantic and Eastern North Pacific basins and the U.S. Department of Defense Joint Typhoon Warning

Center for all other basins, as compiled by the International Best Track Archive for Climate Stewardship (IBTrACS; Knapp, Kruk, et al., 2010) from 1980–2016. Observed intensities are recorded with a precision of five knots, so the lifetime maximum intensity (LMI) is often located at more than one point along the TC track. In this study, the very first point at which the LMI occurs along the track is used, following Wing et al. (2007), referred to here as "actual intensity" (AI). All points except landfall points are retained; if points poleward of 30° latitude are excluded, the results are qualitatively similar (Text S5 and Figures S12–S19 in the supporting information).

Several reanalysis data sets are used to calculate PI, including the European Centre for Medium-Range Weather Forecasts Interim Reanalysis (ERA-Interim; Dee et al., 2011) and the second Modern-Era Retrospective Analysis for Research and Applications (MERRA-2; Gelaro et al., 2017). Since the calculation of PI may be sensitive to the choice of SST data, calculations were also performed with atmospheric variables from MERRA-2, but with SSTs substituted from the UK Met Office Hadley Centre for Climate Prediction and Research sea ice and sea surface temperature (HadISST1) data set (Rayner et al., 2003)—this version of PI is referred to as "MERRA-2 HadISST" (see Gilford, 2018). Additional sensitivity tests were also conducted using the National Centers for Environmental Prediction/National Center for Atmospheric Research (NCEP/NCAR; Kalnay et al., 1996) and the ECMWF Atmospheric Reanalysis of the 20th Century (ERA-20C; Stickler et al., 2014) reanalyses.

3. Methodology

PI is dependent on both the enthalpy difference between the sea surface and atmosphere and the temperature difference between the sea surface and the TC outflow level (approximately the tropopause; Emanuel et al., 2013) and is given by Bister and Emanuel (1998) as

$$V_{max}^2 = \frac{C_k}{C_D}\frac{T_s - T_o}{T_o}\left(h_o^* - h^*\right), \tag{1}$$

where C_k and C_D are the surface enthalpy and momentum exchange coefficients, T_s is the SST, T_o is the outflow temperature, h_o^* is the saturation moist static energy of the sea surface, and h^* is the saturation moist static energy of the free troposphere (which is assumed to be the same as the boundary layer moist static energy in a deep convecting atmosphere). The thermodynamic efficiency $\left(\frac{T_s - T_o}{T_o}\right)$ is more sensitive to changes in T_o than changes in SST, so SSTs primarily influence PI through the air-sea disequilibrium term $\left(h_o^* - h^*\right)$. It is thus not the absolute value of SST, but the difference between temperatures of the sea surface and the free troposphere that contributes to PI variability (Emanuel et al., 2013).

PI is calculated from monthly reanalysis data following previous studies (e.g., Gilford et al., 2019; Strazzo et al., 2015; Vecchi & Soden, 2007; Wing et al., 2015, 2007) using the BE02 (Bister & Emanuel, 2002) algorithm. While PI may vary on submonthly time scales, using submonthly PI values rather than monthly averages is not expected to affect correlations with actual TC intensity (Kossin, 2015). T_o is calculated as the temperature at the level of neutral buoyancy for a saturated parcel of air, which has been reversibly and adiabatically lifted from sea level pressure, and the $\frac{C_k}{C_D}$ ratio is set to the constant value of 0.9, following previous studies (Gilford et al., 2017; Wang et al., 2014; Wing et al., 2015). The BE02 algorithm is more accurate for PI calculations than directly calculating and multiplying each term on the right-hand side of Equation 1 because the BE02 algorithm accounts for water loading and the virtual temperature effect (Bister & Emanuel, 2002). The calculated T_o and SSTs from each reanalysis are used to calculate the efficiency term. PI, T_o, efficiency, and SSTs for each reanalysis are fit to a common 2.5° × 2.5° grid (Gilford et al., 2017). Given $\frac{C_k}{C_D}$, directly calculated efficiency, and BE02 algorithm-derived PI, the disequilibrium term is calculated as a residual after taking the natural logarithm of Equation 1:

$$2log\left(V_{max}\right) = log\left(\frac{C_k}{C_D}\right) + log\left(\frac{T_s - T_o}{T_o}\right) + log\left(h_o^* - h^*\right). \tag{2}$$

Although Equation 2 is an approximation to the BE02 algorithm, Wing et al. (2015) showed that it is still reasonable to use it to solve for the logarithm of the disequilibrium term as a residual. To test the sensitivity of the results to this approach, the disequilibrium term is also directly calculated using MERRA-2 data with h^* calculated at 500 hPa, representing the midtroposphere. The results are similar when calculating h^* at 600 hPa (Text S4; Tables S2–S13). The values of PI, efficiency, and the logarithm of disequilibrium at the

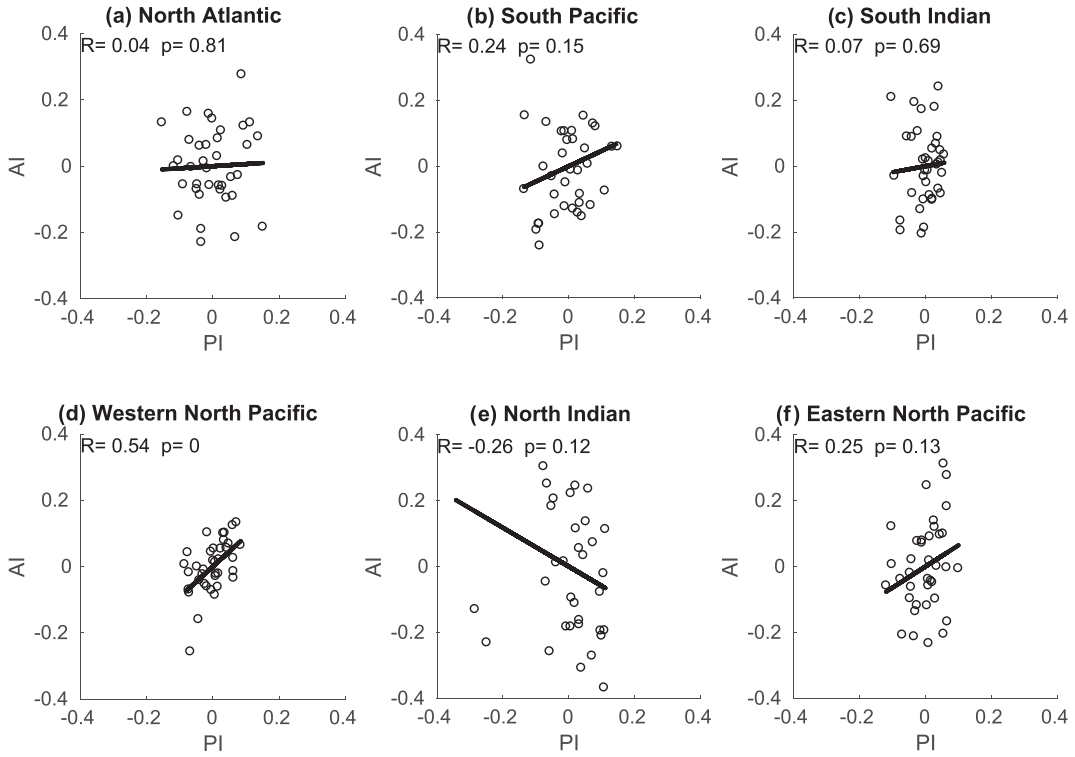

Figure 1. Scatter plots of AI versus PI for each basin for the set of tropical storms and hurricanes including AI > PI from ERA-Interim for 1980–2016. These correlations are representative of the other reanalyses and sets. *R* is the correlation coefficient, and *p* is the *p* value. The black line is a linear best fit line. The data have been normalized and detrended.

location and month in which the TC first reached its LMI ("AI") are extracted for each storm in a given basin from 1980–2016; this PI is referred to as "along-track PI," as opposed to the basin-averaged PI that is considered in many other studies. Next, these variables are averaged over all storms in each year so that there is one average AI and PI value per year.

In order to separate the influence of SST and T_o on variability in the efficiency term, two additional versions of the efficiency term are computed—one that uses monthly climatological values of SST but varying T_o and one that uses monthly climatological values of T_o but varying SST. For example, the logarithm of efficiency with climatological T_o is given by

$$log(\text{eff}_{climo\,T_o}) = log\left(\frac{T_s(t) - \langle T_o\rangle}{\langle T_o\rangle}\right). \tag{3}$$

In Equation 3, $T_s(t)$ is the SST of the specific month of AI while $\langle T_o\rangle$ is the monthly climatological value of T_o averaged over 1980–2016. Equation 3 represents the SST contribution to efficiency variability. Similarly,

$$log(\text{eff}_{climo\,T_s}) = log\left(\frac{\langle T_s\rangle - T_o(t)}{T_o(t)}\right) \tag{4}$$

represents the T_o contribution to efficiency variability.

We consider three sets of storms in our analyses. The first set contains tropical storms and hurricanes and includes gridpoints where AI is greater than PI, which may occur due to, for instance, limitations of PI theory (e.g., Bryan & Rotunno, 2009). Including this set also allows us to directly compare results to Wing et al. (2007). The second set includes only TCs reaching hurricane strength during their lifetime and includes gridpoints where AI > PI. The third set consists of tropical storms and hurricanes but excludes gridpoints where AI > PI.

Table 1
AI Versus PI Correlation Statistics

Set	*R*	*p* value
Western North Pacific		
MERRA-2 HadISST		
Hurricanes including AI > PI	**0.57**	**<0.01**
TS/hurricanes including AI > PI	**0.44**	**0.01**
TS/hurricanes excluding AI >PI	**0.53**	**<0.01**
MERRA-2		
Hurricanes including AI > PI	**0.73**	**<0.01**
TS/hurricanes including AI > PI	**0.57**	**<0.01**
TS/hurricanes excluding AI >PI	**0.37**	**0.03**
ERA-Interim		
Hurricanes including AI > PI	**0.64**	**<0.01**
TS/hurricanes including AI > PI	**0.54**	**<0.01**
TS/hurricanes excluding AI >PI	**0.62**	**<0.01**
North Atlantic		
MERRA-2 HadISST		
Hurricanes including AI > PI	0.17	0.30
TS/hurricanes including AI > PI	0.20	0.23
TS/hurricanes excluding AI >PI	0.22	0.18
MERRA-2		
Hurricanes including AI > PI	0.19	0.26
TS/hurricanes including AI > PI	−0.04	0.80
TS/hurricanes excluding AI >PI	0.18	0.29
ERA-Interim		
Hurricanes including AI > PI	0.11	0.53
TS/hurricanes including AI > PI	0.04	0.81
TS/hurricanes excluding AI >PI	0.24	0.16

Note. Results for the Western North Pacific and North Atlantic, for 1980–2016. The correlation coefficients (*R*) and *p* values between AI and PI are displayed. Values are in bold if significant at the 95% confidence level.

To examine correlations between AI and PI, yearly averaged AI and PI are normalized by their respective climatological average over all years according to

$$PI_{norm} = \frac{\langle PI \rangle_{yearly} - \langle PI \rangle_{climo}}{\langle PI \rangle_{climo}} \tag{5}$$

and likewise for AI. The time series of normalized AI and PI are then detrended by subtracting the linear best fit line. The correlation coefficient between time series of normalized and detrended AI and PI is considered to be statistically significant at the 95% confidence level using the student's *t* test.

4. Relationship Between AI and PI Variability

4.1. Correlation Results

Figure 1 summarizes the results from ERA-Interim over 1980–2016 for each basin, for the set of tropical storms and hurricanes including grid points where AI > PI. In each basin, AI variability tends to be larger than PI variability, but the Western North Pacific is the only basin with a statistically significant correlation between AI and PI (Figure 1). This conclusion is robust across other reanalyses and sets of storms; for all other basins, nearly all reanalysis/set combinations have insignificant correlations (Text S1; Figures S1–S6).

The correlations in the Western North Pacific range from $R = 0.37$ to $R = 0.73$, depending on the data set and set, all of which are significant at the 95% confidence level (Table 1; Figure S5). These results reflect

a strong correspondence between the variability of AI and PI and are consistent with Wing et al. (2007), though the correlations found here are generally higher.

The North Indian ocean basin has a single statistically significant correlation of $R = -0.34$, for the sets of tropical storms and hurricanes including AI > PI from MERRA-2 HadISST (Figure S2). This and other (nonsignificant) negative correlations in the North Indian (Figure 1e) are most likely related to the low number of TCs that occur in this basin and the modulation of TC activity by other factors like wind shear associated with the monsoon circulation (Gilford et al., 2019). The South Pacific and South Indian have no significant correlations between AI and PI in any of the sets or data sets considered (Figures 1b, 1c, S3, and S4). In the Eastern North Pacific, the set of hurricanes including AI > PI has statistically significant correlations between AI and PI in MERRA-2 and MERRA-2 HadISST ($R = 0.47$, $R = 0.46$), and a nearly significant correlation ($R = 0.33$, $p = 0.05$) in ERA-Interim (Figures 1f and S6).

As shown in Table 1, no statistically significant correlations between AI and PI are found for the North Atlantic (see also Figures 1a and S1). This is in contrast to Wing et al. (2007), who found statistically significant correlations in the North Atlantic. The reasons for this inconsistency are investigated in the next section.

4.2. Sensitivity to Data Set and Time Period

The analysis in this study differs from that of Wing et al. (2007) in both the choice of data set and time period; Wing et al. (2007) considered the 56-year time period of 1950–2005 and the NCEP/NCAR reanalysis while we consider the 37-year time period of 1980–2016 and MERRA-2, MERRA-2 HadISST, and ERA-Interim reanalyses. We repeat our analysis of the North Atlantic from 1980–2016 using NCEP/NCAR reanalysis to calculate PI. This also yields insignificant results (Text S2; Figure S7), indicating that the inconsistency between our results and Wing et al. (2007) does not arise from the choice of data set. To probe the sensitivity of correlations between AI and PI to the time period considered, we subset the NCEP/NCAR reanalysis data from 1950–2016 into all possible combinations of periods of 10-, 20-, 30-, 34-, 37-, 40-, 45-, 56-, 60-, and 67-year lengths (Figures 2 and S8; Text S3). For years before 1979, 1.9 m/s is subtracted from all PI values to account for discontinuities due to the introduction of satellite data (Emanuel, 2007; Wing et al., 2007). Qualitatively similar results are obtained when using the ERA-20C reanalysis from 1950–2010 (Figure S9); results from NCEP/NCAR are shown here for comparison to Wing et al. (2007). The analysis considering the set of hurricanes including AI > PI is shown in Figure 2, in which the correlation coefficient and corresponding p value are plotted for each time period considered.

As the number of years in the time period increases, both the average correlation and fraction of correlations that are statistically significant increase. There are a wide range of correlations in the 10- and 20-year time periods, but none are statistically significant, reflecting short, noisy time series. Ten percent of the 30- and 34-year time periods have significant correlations, while 20% of the 37-year time periods do (not including the 1980–2016 period considered here, which has the lowest correlation of the 37-year time periods). For the 40-, 45-, and 50-year time periods, 30%, 50%, and 80% have significant correlations, respectively. All 56-, 60-, and 67-year time periods yield statistically significant correlations between AI and PI, including the 1950–2005 period considered by Wing et al. (2007).

It is clear that the discrepancy between our results for the North Atlantic and those of Wing et al. (2007) arises due to the different time period used. For a short time period, a larger correlation than the typical $R \sim 0.2$–0.4 observed would be needed for it to be statistically significant. The correlation between AI and PI is not only influenced by the number of years in the sample size, but also the specific years included, with a larger spread of possible correlations for shorter time series. There is no obvious pattern to how the value of the correlation depends on the central year of the time period considered, except for a slight tendency for correlations covering years later in the record to be lower (Figure S10). The same sensitivity tests are also performed for the Western North Pacific, where there is a significant correlation in most time periods tested (Text S3; Figures S8 and S9). We speculate on the reason for the particular sensitivity of the AI versus PI relationship to the time period examined in the North Atlantic in the conclusions.

5. Factors Contributing to PI and AI Interannual Variability

5.1. Role of Efficiency in PI Variability

Next, we investigate the contributions of thermodynamic efficiency and air-sea disequilibrium to PI variability. This follows from Wing et al. (2015), who found that 20–71% of the interannual variance in

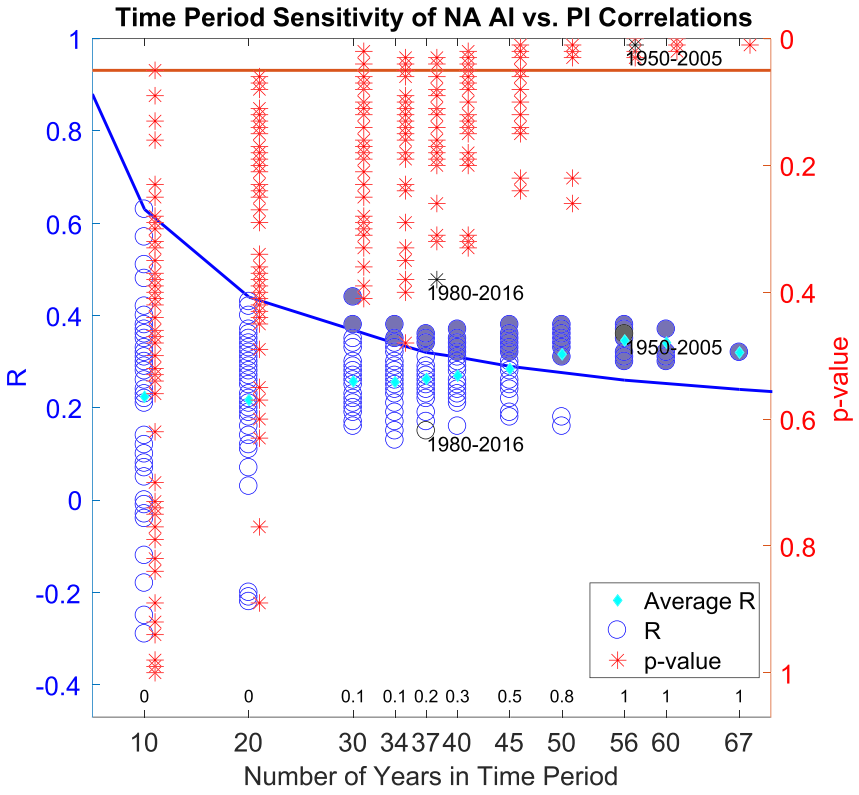

Figure 2. Correlation coefficients between AI and PI (R, on the left y axis and blue circles) and p values (on the right y axis and red asterisks) for all combinations of years in a time period of a given length, for the set of hurricanes including AI > PI from NCEP/NCAR in the North Atlantic. The correlation coefficients and p values for each time period length are offset from each other for visual clarity. The red line indicates a p value of 0.05 (statistical significance at the 95% confidence level). The blue line indicates the correlation coefficient that would be required to have a statistically significant correlation given that number of years. The filled blue circles (correlation coefficients) above this line are the cases that are statistically significant. The fraction of cases that are significant is indicated by the text above the x-axis label for each time period length. The cyan diamonds indicate the average correlation coefficient for each length of time period. The time periods considered in this study (1980–2016) and in Wing et al. (2007) (1950–2005) are labeled in black.

basin-averaged PI was explained by variability in efficiency, but here we examine PI sampled along actual TC tracks. High and significant correlations (most at the 99% confidence level) are observed between detrended time series of efficiency and PI for all cases (shown in Table 2 for the set of hurricanes including AI > PI from MERRA-2; see Tables S2, S4, S6, S8, S10, and S12 for others). To some extent, high correlations were expected since PI directly depends on efficiency (Equation 1), but since PI also depends on other factors, these correlations are still notable. The highest correlation between efficiency and PI is for the set of hurricanes including AI > PI from MERRA-2 HadISST in the North Indian, which has a correlation coefficient of $R = 0.98$ (Table S4). When considering all sets and data sets, the North Atlantic has the highest correlations between efficiency and PI of any basin, consistent with Wing et al. (2015), who found larger contributions of efficiency to PI trends in that basin (Table S2).

The differences between the correlations with PI of efficiency calculated using climatological SST and efficiency calculated using climatological T_o are not statistically significant at the 95% level (based on a two-sided Z test), with the exception of the set of hurricanes including AI > PI in MERRA-2 in the North Indian. In this case, efficiency using climatological SST is more strongly correlated with PI (Table 2). Otherwise, both T_o and SST contribute to efficiency-driven PI variability. While not statistically significant, T_o is generally a greater factor in the North Atlantic, Western North Pacific, and Eastern North Pacific (Tables S2, S10, and S12), and SST is generally a greater factor in the South Indian and South Pacific (Tables S6 and S8). Comparing the reanalyses, T_o tends to be a greater contributor to efficiency-driven PI variability in MERRA-2 (Table 2) while the contribution from SST plays a bigger role in ERA-Interim and MERRA-2 HadISST (Text S4; Tables S2, S4, S6, S8, S10, and S12).

Table 2
Factors Contributing to PI and AI Variability

Term versus PI	R	R^2	p value
	North Atlantic		
Direct disequilibrium	**0.62**	**0.38**	**<0.01**
Residual disequilibrium	**0.69**	**0.48**	**<0.01**
Efficiency	**0.97**	**0.94**	**<0.01**
Efficiency climo T_o	**0.95**	**0.90**	**<0.01**
Efficiency climo T_s	**0.97**	**0.94**	**<0.01**
	North Indian		
Direct disequilibrium	0.37	0.14	0.06
Residual disequilibrium	**0.99**	**0.98**	**<0.01**
Efficiency	**0.98**	**0.96**	**<0.01**
Efficiency climo T_o	**0.94**	**0.88**	**<0.01**
Efficiency climo T_s	**0.98**	**0.96**	**<0.01**
	South Indian		
Direct disequilibrium	**0.77**	**0.59**	**<0.01**
Residual disequilibrium	**0.96**	**0.92**	**<0.01**
Efficiency	**0.63**	**0.40**	**<0.01**
Efficiency climo T_o	**0.76**	**0.58**	**<0.01**
Efficiency climo T_s	**0.62**	**0.38**	**<0.01**
	South Pacific		
Direct disequilibrium	**0.72**	**0.52**	**<0.01**
Residual disequilibrium	**0.96**	**0.92**	**<0.01**
Efficiency	**0.78**	**0.61**	**<0.01**
Efficiency climo T_o	**0.82**	**0.67**	**<0.01**
Efficiency climo T_s	**0.76**	**0.58**	**<0.01**
	Western North Pacific		
Direct disequilibrium	**0.75**	**0.56**	**<0.01**
Residual disequilibrium	**0.93**	**0.86**	**<0.01**
Efficiency	**0.86**	**0.74**	**<0.01**
Efficiency climo T_o	**0.68**	**0.46**	**<0.01**
Efficiency climo T_s	**0.85**	**0.72**	**<0.01**
	Eastern North Pacific		
Direct disequilibrium	**0.79**	**0.62**	**<0.01**
Residual disequilibrium	**0.99**	**0.98**	**<0.01**
Efficiency	**0.86**	**0.74**	**<0.01**
Efficiency climo T_o	**0.67**	**0.45**	**<0.01**
Efficiency climo T_s	**0.83**	**0.69**	**<0.01**

(Continued)

Across all basins, reanalyses, and sets of TCs, the variance in efficiency explains 10–96% of interannual variability in along-track PI, T_o-driven efficiency variations explain 7–96%, and SST-driven efficiency variations explain 14–90%. The correlations between efficiency and PI found here for along-track PI are in general larger than those found for basin-average PI in Wing et al. (2015). This indicates that the variability in PI and its constituents are different in the locations sampled by TCs at their LMI than variability averaged over the regions of peak TC activity, but an explanation for this requires investigating track variability in more detail.

5.2. Role of Disequilibrium in PI Variability

Extremely high correlations between detrended disequilibrium (computed as a residual) and PI are found for all cases, all significant at the 99% confidence level. There are numerous instances of $R = 0.99$, most

Table 2 *(continued)*

Term versus AI	R	R^2	p value
	Western North Pacific		
Direct disequilibrium	**0.47**	**0.22**	**<0.01**
Residual disequilibrium	**0.68**	**0.46**	**<0.01**
Efficiency	**0.65**	**0.42**	**0.03**
Efficiency climo T_o	**0.68**	**0.46**	**0.01**
Efficiency climo T_s	**0.66**	**0.44**	**0.03**
	Eastern North Pacific		
Direct disequilibrium	0.15	0.02	0.37
Residual disequilibrium	**0.41**	**0.17**	**0.01**
Efficiency	**0.54**	**0.29**	**0.01**
Efficiency climo T_o	**0.39**	**0.15**	**0.02**
Efficiency climo T_s	**0.53**	**0.28**	**0.01**

Note. Results are shown for the case of hurricanes including AI > PI from MERRA-2 for each basin that has statistically significant correlations. Values are in bold if significant at 95%, and terms with the largest R^2 for each basin are italicized. Direct disequilibrium uses 500 hPa to calculate h^*.

consistently in the set with hurricanes including AI > PI in the East Pacific and South Pacific (see Table 2 for MERRA-2; also Tables S8 and S12). High correlations were expected because disequilibrium is calculated as a residual from Equation 2, which directly connects disequilibrium to PI. Statistically significant, but lower, correlations are also found when disequilibrium is calculated directly (using either 500 or 600 hPa for the h^* calculation) using MERRA-2 in all basins except the North Indian.

When calculated as a residual, disequilibrium is more strongly correlated with PI than efficiency is in all of the cases with a statistically significant difference in correlations, which represent 83% of the total cases (across all basins and reanalyses). However, efficiency is more strongly correlated with PI than directly calculated disequilibrium is in all but one of the cases for which there is a statistically significant difference, which represent half of the total cases. Therefore, it is difficult to come to a robust conclusion on the relative roles of SST and T_o in PI variability, as (statistically) both contribute and the dominant factor depends on how disequilibrium is calculated. Note that Wing et al. (2015) and Gilford et al. (2017) found that SST was the main factor in trends and the seasonal cycle of PI in most basins.

5.3. Role of Efficiency and Disequilibrium in AI Variability

Overall, it is expected that if there is a significant correlation between PI and AI (cf. section 4), then at least one of the components of PI should also have a significant correlation with AI. Indeed, in the Western North Pacific, disequilibrium and efficiency are both correlated with AI variability (shown in Table 2 for the set of hurricanes including AI > PI from MERRA-2; see Table S11 for others). On the other hand, there are several cases that do not have a statistically significant AI versus PI correlation yet contain a statistically significant correlation between AI and efficiency and/or disequilibrium. For example, for the set of hurricanes including AI > PI in the East Pacific, there is a significant correlation between efficiency and AI in all three data sets (Tables 2 and S13). This indicates that a lack of significant correlation between AI and PI could result from inconsistent behavior in the factors contributing to PI variability.

6. Conclusions

Unlike many other studies that have focused on basin-averaged PI trends (Emanuel et al., 2013; Gilford et al., 2017; Wing et al., 2015) or the influence of SSTs on TC intensity (Holland & Bruyere, 2014; Knutson et al., 2010; Strazzo et al., 2015; Walsh et al., 2016), this study analyzed the relationship between interannual variability in along-track PI and AI as well as the relative contributions of thermodynamic efficiency and air-sea disequilibrium to that variability.

Based on previous empirical results linking AI variability to PI variability (Emanuel, 2000; Wing et al., 2007), a positive, statistically significant correlation between AI and PI was expected. However, the Western

North Pacific is the only basin to consistently yield such correlations over the time period from 1980–2016, across the multiple reanalyses and sets of TCs considered. This result contrasts with the findings of Wing et al. (2007) in which both the Western North Pacific and North Atlantic had significant correlations. This lack of agreement is due to the different time periods examined. Consistent with expectations, PI theory holds best in the Western North Pacific, because of its large number of intense TCs and strong thermodynamic modulation of TC activity. A variety of complicating factors in the other basins may prevent a statistically significant relationship between AI and PI from emerging: The North Atlantic has substantial multidecadal variability, which may contribute to the sensitivity of the results to the time period (Goldenberg et al., 2001; Vimont & Kossin, 2007); TC activity in the North Indian is strongly modulated by other factors like the monsoon circulation (Camargo et al., 2010; Evan & Camargo, 2011; Gray, 1968); the historical TC data are known to be especially flawed in the Southern Hemisphere even as recently as 1985 (Ramsay, 2017; Schreck et al., 2014); and the TC activity in the Eastern North Pacific is densely contained in a small region (Gray, 1968).

It is worth further considering why the results are so sensitive to both the length of the time period and the specific years. In addition to longer records having greater sample sizes (making it easier to achieve statistical significance), a long time series with its linear trend removed contains both interannual and interdecadal to multidecadal variability. A preliminary analysis of the correlation between AI and PI in the North Atlantic reveals that the correlation is much higher when a running average over >5 years is applied to the time series (Text S3; Figure S11; Table S1). This indicates that AI variability is more strongly controlled by PI variability on longer time scales. Thus, the AI versus PI relationship may only emerge when lower-frequency variability is present in the time series, as it was in the time series considered by Wing et al. (2007). In addition, several anomalous storms in an individual year may bias the AI versus PI relationship, which could explain why some time periods of a given length have a significant correlation and others do not. North Atlantic correlations may be more susceptible to this than in the western North Pacific because there are far fewer storms in the Atlantic (Gilford et al., 2019). While the number of TCs in a given year does not directly affect the p value for correlations between annual mean time series, it affects how representative the annual mean AI and PI values are. Through the principle of error propagation, uncertainty in the annual mean (which would be larger in the years with fewer TCs) leads to uncertainty in the value of the correlation coefficient, which in turn affects the p value and therefore statistical significance of the correlation. Future work could investigate these possible reasons for the lack of correlation between AI and PI on short time scales in more detail.

Both efficiency and disequilibrium contribute to variations in along-track PI. Variability in the various versions of the efficiency term explains 7–96% of along-track PI variability, while variability in disequilibrium explains 48–98%. This large spread in variance explained illustrates how basin and data set can affect the interpretation of which factor is most important for PI variability. Overall, disequilibrium calculated as a residual has the highest correlations with both PI and AI, emphasizing the role of SSTs in TC intensity variability, but outflow temperature also plays a role. The lack of correlations between AI and PI in many basins suggest that factors not considered in PI theory, such as vertical wind shear, the entrainment of dry air, and ocean-atmosphere interaction, should also be considered in the year-to-year variability of actual TC intensity.

Data Availability Statement

The IBTrACS data were obtained from NOAA's National Climatic Data Center available at https://doi.org/10.7289/V5NK3BZP (Knapp, Applequist, et al., 2010). The MERRA-2 data were obtained from NASA's Global Modeling and Assimilation Office (GMAO) at https://doi.org/10.5067/A7S6XP56VZWS (Global Modeling and Assimilation Office, 2015). The ERA-Interim data were obtained from ECWMF at https://apps.ecmwf.int/datasets/data/interim-full-daily. The NCEP/NCAR and ERA-20C data are available from the Research Data Archive at the National Center for Atmospheric Research, available at https://rda.ucar.edu/datasets/ds090.0/ (NCEP/NWS/NOAA/U.S. Department of Commerce, 1994) and https://doi.org/10.5065/D6VQ30QG (ECMWF, 2014), respectively. The HadISST1 data were obtained from the UK Met Office Hadley Centre for Climate Prediction and Research at http://www.metoffice.gov.uk/hadobs/hadisst/data/download.html. The code to calculate potential intensity is available at ftp://texmex.mit.edu/pub/emanuel/TCMAX/pcmin.m, courtesy of Kerry Emanuel. The along-track potential intensity data is available at https://doi.org/10.5281/zenodo.3905132 (Gilford et al., 2020).

Acknowledgments
A. A. W. was supported by the NOAA Climate Program Office's Modeling, Analysis, Predictions, and Projections program under Grant NA18OAR4310270. D. G. was supported by NSF Grant ICER-1663807 and NASA Grant 80NSSC17K069. We thank Dr. Suzana Camargo for sharing the potential intensity data calculated from the NCEP/NCAR and ERA-20C reanalyses. The first author thanks Dr. Robert Hart and Dr. Philip Sura for research advice and support.

References

Bister, M., & Emanuel, K. A. (1998). Dissipative heating and hurricane intensity. *Meteorology and Atmospheric Physics*, *52*, 233–240.
Bister, M., & Emanuel, K. A. (2002). Low frequency variability of tropical cyclone potential intensity 1. Interannual to interdecadal variability. *Journal of Geophysical Research*, *107*(D24), 4801. https://doi.org/10.1029/2001JD000776
Bryan, G. H., & Rotunno, R. (2009). Evaluation of an analytical model for the maximum intensity of tropical cyclones. *Journal of the Atmospheric Sciences*, *66*, 3042–3060. https://doi.org/10.1175/2009JAS3038.1
Camargo, S. J. (2013). Global and regional aspects of tropical cyclone activity in the CMIP5 models. *Journal of Climate*, *26*(24), 9880–9902. https://doi.org/10.1175/JCLI-D-12-00549.1
Camargo, S. J., Sobel, A. H., Barnston, A. G., & Klotzbach, P. J. (2010). Global perspectives on tropical cyclones: From science to mitigation. In J. C. L. Chan, & J. D. Kepert (Eds.), *World Scientific Series on Asia-Pacific Weather and Climate* (Vol. 4, pp. 325–360). Singapore: World Scientific Publishing.
Camargo, S. J., Ting, M., & Kushnir, Y. (2013). Influence of local and remote SST on North Atlantic tropical cyclone potential intensity. *Climate Dynamics*, *40*, 1515–1529. https://doi.org/10.1007/s00382-012-1536-4
Dee, D. P., Uppala, S. M., Simmons, A. J., Berrisford, P., Poli, P., Kobayashi, S., et al. (2011). The ERA-interim reanalysis: Configuration and performance of the data assimilation system. *Quarterly Journal of the Royal Meteorological Society*, *137*, 553–597. https://doi.org/10.1002/qj.828
ECMWF (2014). ERA-20C Project (ECMWF Atmospheric Reanalyses of the 20th Century). Research Data Archive at the National Center for Atmospheric Research, Computational and Information Systems Laboratory. https://doi.org/10.5065/D6VQ30QG
Emanuel, K. (1986). An air-sea interaction theory for tropical cyclones. Part I: Steady-State maintenance. *Journal of the Atmospheric Sciences*, *43*(6), 585–605.
Emanuel, K. (2000). A statistical analysis of tropical cyclone intensity. *Monthly Weather Review*, *128*(4), 1139–1152.
Emanuel, K. (2007). Environmental factors affecting tropical cyclone power dissipation. *Journal of Climate*, *20*, 5497–5509.
Emanuel, K. (2015). Effect of upper-ocean evolution on projected trends in tropical cyclone activity. *Journal of Climate*, *28*(20), 8165–8170. https://doi.org/10.1175/JCLI-D-15-0401.1
Emanuel, K., & Sobel, A. (2013). Response of tropical sea surface temperature, precipitation, and tropical cyclone-related variables to changes in global and local forcing. *Journal of Advances in Modeling Earth Systems*, *5*, 447–458. https://doi.org/10.1002/jame.20032
Emanuel, K., Solomon, S., Folini, D., Davis, S., & Cagnazzo, C. (2013). Influence of tropical tropopause layer cooling on atlantic hurricane activity. *Journal of Climate*, *26*(7), 2288–2301. https://doi.org/10.1175/JCLI-D-12-00242.1
Evan, A. T., & Camargo, S. J. (2011). A climatology of Arabian Sea cyclonic storms. *Journal of Climate*, *24*, 140,178.
Free, M., Bister, M., & Emanuel, K. (2004). Potential intensity of tropical cyclones: Comparison of results from radiosonde and reanalysis data. *Journal of Climate*, *17*(8), 1722–1727. https://doi.org/10.1175/1520-0442(2004)017<1722:PIOTCC>2.0.CO;2
Gelaro, R., McCarty, W., Suarez, M. J., Todling, R., Molod, A., Takacs, L., et al. (2017). The Modern-Era Retrospective Analysis for Research and Applications, Version 2 (MERRA-2). *Journal of Climate*, *30*, 5419–5454. https://doi.org/10.1175/jcli-d-16-0758.1
Gilford, D. M. (2018). The tropopause region thermal structure and tropical cyclones (Ph.D. Thesis), Massachusetts Institute of Technology.
Gilford, D. M., Solomon, S., & Emanuel, K. A. (2017). On the seasonal cycles of tropical cyclone potential intensity. *Journal of Climate*, *30*(16), 6085–6096. https://doi.org/10.1175/JCLI-D-16-0827.1
Gilford, D. M., Solomon, S., & Emanuel, K. (2019). Seasonal cycles of along-track tropical cyclone maximum intensity. *Monthly Weather Review*, *147*, 2417–2432. https://doi.org/10.1175/MWR-D-19-0021.1
Gilford, D. M., Wing, A., & Shields, S. (2020). Tropical cyclone along-track potential intensity (and derived quantities) for six ocean basins from three reanalyses, 1980–2016 (Version 1.1). Zenodo. Retrieved from https://doi.org/10.5281/zenodo.3905132
Global Modeling and Assimilation Office (GMAO) (2015), MERRA-2 inst6_3d_ana_Np: 3d,6-Hourly, Instantaneous,Pressure-Level,Analysis,Analyzed Meteorological Fields V5.12.4, Greenbelt, MD, USA, Goddard Earth Sciences Data and Information Services Center (GES DISC), Retrieved from https://doi.org/10.5067/A7S6XP56VZWS
Goldenberg, S. B., Landsea, C. W., Mestas-Nunez, A. M., & Gray, W. M. (2001). The recent increase in Atlantic hurricane activity: Causes and implications. *Science*, *293*, 474179.
Gray, W. M. (1968). Global view of the origin of tropical disturbances and storms. *Monthly Weather Review*, *96*, 669,170.
Holland, G. J., & Bruyere, C. L. (2014). Recent intense hurricane response to global climate change. *Climate Dynamics*, *42*, 617–627. https://doi.org/10.1007/s00382-013-1713-0
Huang, P., Lin, I.-I., Chou, C., & Huang, R.-H. (2015). Change in ocean subsurface environment to suppress tropical cyclone intensification under global warming. *Nature Communications*, *6*, 7188.
Kalnay, E., Kanamitsu, M., Kistler, R., Collins, W., Deaven, D., Gandin, L., et al. (1996). The NCEP/NCAR 40-year reanalysis project. *Bulletin of the American Meteorological Society*, *77*(3), 437–471. https://doi.org/10.1175/1520-0477(1996)077<0437:TNYRP>2.0.CO;2
Knapp, K. R., Applequist, S., Diamond, H. J., Kossin, J. P., Kruk, M., & Schreck, C. (2010). NCDC International Best Track Archive for Climate Stewardship (IBTrACS) Project, Version 3. [v03r10]. NOAA National Centers for Environmental Information. Retrieved from https://doi.org/10.7289/V5NK3BZP
Knapp, K. R., Kruk, M. C., Levinson, D. H., Diamond, H. J., & Neumann, C. J. (2010). The International Best Track Archive for Climate Stewardship (IBTrACS): Unifying tropical cyclone data. *Bulletin of the American Meteorological Society*, *91*(3), 363–376. https://doi.org/10.1175/2009BAMS2755.1
Knutson, T. R., McBride, J. L., Chan, J., Emanuel, K., Holland, G., Landsea, C., et al. (2010). Tropical cyclones and climate change. *Nature Geoscience*, *3*, 157–163. https://doi.org/10.1038/ngeo779
Kossin, J. P. (2015). Validating atmospheric reanalysis data using tropical cyclones as thermometers. *Bulletin of the American Meteorological Society*, *96*, 1089–1096. https://doi.org/10.1175/BAMS-D-14-00180.1
Kossin, J. P., & Camargo, S. J. (2009). Hurricane track variability and secular potential intensity trends. *Climatic Change*, *97*, 329–337. https://doi.org/10.1007/s10584-009-9748-2
Lin, I.-I., Black, P., Price, J. F., Yang, C.-Y., Chen, S. S., Lien, C.-C., et al. (2013). An ocean coupling potential intensity index for tropical cyclones. *Geophysical Research Letters*, *40*, 1878–1882. https://doi.org/10.1002/grl.50091
NCEP/NWS/NOAA/U.S. Department of Commerce (1994). NCEP/NCAR Global Reanalysis Products, 1948-continuing. Research Data Archive at the National Center for Atmospheric Research, Computational and Information Systems Laboratory. Retrieved from https://rda.ucar.edu/datasets/ds090.0/
Polvani, L. M., Camargo, S. J., & Garcia, R. R. (2016). The importance of the Montreal Protocol in mitigating the potential intensity of tropical cyclones. *Journal of Climate*, *29*, 2275–2289. https://doi.org/10.1175/JCLI-D_15-0232.1
Ramsay, H. A. (2013). The effects of imposed stratospheric cooling on the maximum intensity of tropical cyclones in axisymmetric Radiative-Convective equilibrium. *Journal of Climate*, *26*(24), 9977–9985. https://doi.org/10.1175/JCLI-D-13-00195.1

Ramsay, H. A. (2017). *The global climatology of tropical cyclones*: Oxford Research Encyclopedia of Natural Hazard Science. https://doi.org/10.1093/acrefore/9780199389407.013.79

Rayner, N. A., Parker, D. E., Horton, E. B., Folland, C. K., Alexander, L. V., Rowell, D. P., et al. (2003). Global analyses of sea surface temperature, sea ice, and night marine air temperature since the late nineteenth century. *Journal of Geophysical Research*, *108*, 4407. https://doi.org/10.1029/2002JD002670

Schreck, I. I. I., Knapp, K. R., & Kossin, J. P. (2014). The impact of best track discrepancies on global tropical cyclone climatologies using IBTrACS. *Monthly Weather Review*, *142*, 3881–3899. https://doi.org/10.1175/MWR-D-14-00021.1

Sobel, A. H., Camargo, S. J., Hall, T. M., Lee, C., Tippett, M. K., & Wing, A. A. (2016). Human influence on tropical cyclone intensity. *Science*, *353*(6296), 242–246.

Stickler, A. S. B., Valente, M. A., Bethke, J., Sterin, A., Jourdain, S., Roucaute, E., et al. (2014). ERA-CLIM: Historical surface and upper-air data for future reanalyses. *Bulletin of the American Meteorological Society*, *95*, 1419–1430. https://doi.org/10.1175/BAMS-D-13-00147.1

Strazzo, S. E., Elsner, J. B., & LaRow, T. E. (2015). Quantifying the sensitivity of maximum, limiting, and potential tropical cyclone intensity to SST: Observations versus the FSU/COAPS global climate model. *Journal of Advances in Modeling Earth Systems*, *7*, 586–599. https://doi.org/10.1002/2015MS000432

Tang, B., & Emanuel, K. (2010). Midlevel ventilation's constraint on tropical cyclone intensity. *Journal of the Atmospheric Sciences*, *67*(6), 1817–1830. https://doi.org/10.1175/2010JAS3318.1

Vecchi, G. A., Fueglistaler, S., Held, I. M., Knutson, T. R., & Zhao, M. (2013). Impacts of atmospheric temperature trends on tropical cyclone activity. *Journal of Climate*, *26*(11), 3877–3891. https://doi.org/10.1175/JCLI-D-12-00503.1

Vecchi, G. A., & Soden, B. J. (2007). Effect of remote sea surface temperature change on tropical cyclone potential intensity. *Nature*, *450*, 1066–1070.

Vimont, D. J., & Kossin, J. P. (2007). The Atlantic Meridional Mode and hurricane activity. *Geophysical Research Letters*, *34*, L07709. https://doi.org/10.1029/2007GL029683

Walsh, K. J. E., McBride, J. L., Klotzbach, P. J., Camargo, S. J., Holland, G., Knutson, T. R., et al. (2016). Tropical cyclones and climate change. *Wiley Interdisciplinary Reviews: Climate Change*, *7*, 65–89. https://doi.org/10.1002/wcc.371

Wang, S., Camargo, S. J., Sobel, A. H., & Polvani, L. M. (2014). Impact of the tropopause temperature on the intensity of tropical cyclones: An idealized study using a mesoscale model. *Journal of the Atmospheric Sciences*, *71*, 4333–4348. https://doi.org/10.1175/JAS-D-14-0029.1

Wing, A. A., Emanuel, K., & Solomon, S. (2015). On the factors affecting trends and variability in tropical cyclone potential intensity. *Geophysical Research Letters*, *42*, 8669–8677. https://doi.org/10.1002/2015GL066145

Wing, A. A., Sobel, A. H., & Camargo, S. J. (2007). Relationship between the potential and actual intensities of tropical cyclones on interannual time scales. *Geophysical Research Letters*, *34*, L08810. https://doi.org/10.1029/2006GL028581

Yu, J., Wang, Y., & Hamilton, K. (2010). Response of tropical cyclone potential intensity to a global warming scenario in the IPCC AR4 CGCMs. *Journal of Climate*, *23*(6), 1354–1373. https://doi.org/10.1175/2009JCLI2843.1